

A low-rank representation for unsupervised registration of medical images

Dengqiang Jia¹, Shangqi Gao², Qunlong Chen³, Xinzhe Luo², and Xiahai Zhuang^{2,*}

¹ School of Naval Architecture, Ocean and Civil Engineering, Shanghai Jiao Tong University, Shanghai, China,

² School of Data Science, Fudan University, Shanghai,

³ School of Mechanical Engineering, Shanghai Jiao Tong University, Shanghai, China

Abstract. Registration networks have shown great application potentials in medical image analysis. However, supervised training methods have a great demand for large and high-quality labeled datasets, which is time-consuming and sometimes impractical due to data sharing issues. Unsupervised image registration algorithms commonly employ intensity-based similarity measures as loss functions without any manual annotations. These methods estimate the parameterized transformations between pairs of moving and fixed images through the optimization of the network parameters during training. However, these methods become less effective when the image quality varies, e.g., some images are corrupted by substantial noise or artifacts. In this work, we propose a novel approach based on a low-rank representation, i.e., Regnet-LRR, to tackle the problem. We project noisy images into a noise-free low-rank space, and then compute the similarity between the images. Based on the low-rank similarity measure, we train the registration network to predict the dense deformation fields of noisy image pairs. We highlight that the low-rank projection is reformulated in a way that the registration network can successfully update gradients. With two tasks, i.e., cardiac and abdominal intra-modality registration, we demonstrate that the low-rank representation can boost the generalization ability and robustness of models as well as bring significant improvements in noisy data registration scenarios.

1 Introduction

Pair-wise image registration aims at aligning one image to another. Based on the registration, further medical image analysis can be conducted, including image-aided diagnosis, treatment and surgical decision-making. In the last few decades, intensity-based registration methods have experienced extensive development and have been applied successfully to medical image analysis [2, 11, 13, 15, 23, 24, 29]. These traditional registration methods employ intensity-based similarity measures, including intensity difference (e.g., mean square error (MSE)) and correlation-based information (e.g., normalized cross correlation (NCC)), for better performance.

Deep neural networks (DNNs) are powerful in modeling complex functions and thus have been explored for image registration, which have achieved state-of-the-art accuracy [3,6,12,21,25]. Some registration networks do not require ground truth of deformations or manual annotated segmentation, and Balakrishnan et al. [3] named these methods unsupervised registration methods. Unsupervised registration methods formulated the popular similarity measures as loss functions to optimize the network parameters [6, 12, 25].

However, these similarity measures based on intensity differences can have a negative influence on the performance of unsupervised registration networks when substantial noise inevitably occurs in the image. Since generic denoising models assume that noise is separable from the data, a simple idea to solve this problem is to perform registration after image denoising. The two-stage strategy, including denoising and registration, usually requires two individual optimization processes to achieve the optimal solution and may be subject to computationally expensive iterations and parameter combinations.

Since data is inevitably accompanied with noise during the imaging process, denoising becomes essential in computer vision. Owing to the rapid development of optimization techniques, many important denoising algorithms, such as model-based methods [4,5] and learning-based methods [7,9,20], have been well explored. Gu et al. [10] employed low-rank components for image denoising by mining the self-similarity of images.

In this paper, we consider the scenario in which noisy images need to be registered. To the end, we propose an unsupervised image registration framework based on a low-rank representation, referred to as Regnet-LRR. The model builds a novel loss function by computing the similarity between images in a low-rank space. A convolutional neural network (CNN) is employed to achieve efficient optimization of the registration parameters. Besides, Regnet-LRR performs registration of noisy images directly, thus avoiding performing registration after denoising.

The main contributions of this work are three-fold. First, we resolve the problem of unsupervised registration for noisy images in an one-stage framework. Second, we propose a novel loss function for registration which is derived from the low-rank theories. Third, by mapping the noisy images into low-rank space, our model outperforms previous intensity-based ones in pair-wise registration of noisy medical images.

Related work. Intensity variations between images make registration difficult. To address the problem, a general approach to registration is to employ similarity measures that are robust to those intensity variations. These measures can be assumed as a functional or statistical intensity distribution, rather than an identical one. Such robust results have been achieved by building on intensity differences and computing image gradient histograms with a wide range of features such as SIFT [17] and GLOH [19]. However, these methods are sensitive to more intensity variations, such as multiple modalities or substantial noise. To perform registration between multi-modal images, Wachinger et al. [26] mapped images to structural representations that were only dependent on the depicted

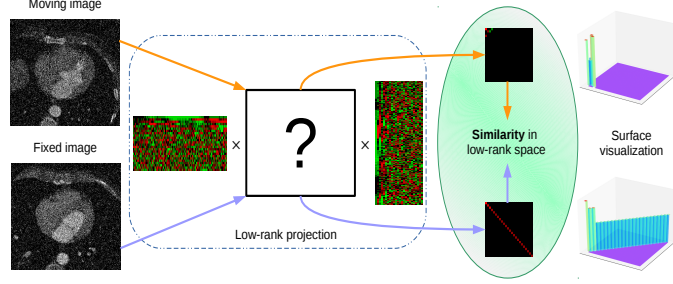


Fig. 1. Schematic illustration of the registration framework with the low-rank representation. In this diagram, the procedure of low-rank projection of the noisy image pair is shown. Subsequently, the registration network is optimized with the similarity measure in the low-rank space.

structures instead of the intensities. However, the design and construction of a noise-free representation for improving medical image registration networks in medical imaging has not been explored in depth.

2 Methods

A noisy intensity image can be considered as $I : \Omega_I \rightarrow \mathbb{R}$, where $\Omega_I \subseteq \mathbb{R}^d$, and d is the dimension of the image domain. Registration of a noisy image pair (I_m and I_f) can be modeled as a mapping from the fixed image domain Ω_{I_f} to the moving image domain Ω_{I_m} by a transformation \mathbf{T} . Suppose Θ is the parameter space for deformation mapping, the mapping \mathbf{T} could then be expressed as the elements in $F = \{\mathbf{T}_\theta | \mathbf{T}_\theta : \Omega_{I_f} \rightarrow \Omega_{I_m}, \theta \in \Theta\}$. An optimal registration can be obtained via the optimization of the following objective function:

$$\hat{\theta} \in \arg \min_{\theta \in \Theta} \mathcal{D}(I_m \circ \mathbf{T}_\theta, I_f) + \lambda \cdot \mathcal{R}(\mathbf{T}_\theta), \quad (1)$$

where $\hat{\theta}$ is an element of the set of deformation parameters, \mathbf{T}_θ is the transformation mapping from the fixed image domain to the moving image domain. In this paper, we assume the transformation \mathbf{T}_θ as the voxel correspondence, which is represented by a dense deformation field (DDF). \mathcal{D} is a similarity measure between two image domains, and $\lambda \cdot \mathcal{R}(\mathbf{T}_\theta)$ is the regularization term with weight λ .

2.1 Image similarity measure in low-rank space

Unsupervised registration is commonly performed based on the similarity measure \mathcal{D} between two images. However, since most of similarity measures are calculated directly in the original image space, they are quite sensitive to substantial noise in the images.

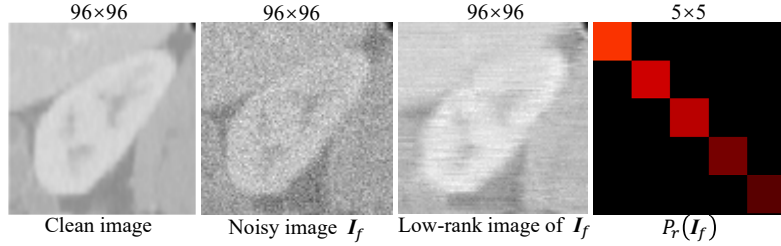


Fig. 2. Visualization of the result of low-rank projection (rank=5) of a noisy image. This noisy image is used as the fixed image in Regnet-LRR. The low-rank projection of the noisy image $P_r(I_f)$ (Section 2.2) is also visualized as an image.

To tackle this problem, we propose the *low-rank projection* method (Section 2.2), which projects images into a noise-free low-rank space at first, and then computes the similarity in the space.

Since low-rank images have excellent self-similarity and noise-free property, we can calculate the image similarity after mapping the images to a low-rank space. Suppose the low-rank component of an image can be obtained by the low-rank projection P_r , where $\text{rank}(P_r(I)) \leq r$, we can then define the image similarity measure $\mathcal{D}_{\mathcal{R}}$ between two images in the low-rank space as follows:

$$\mathcal{D}_{\mathcal{R}}(I_m \circ \mathbf{T}_{\theta}, I_f) = \|P_r(I_m \circ \mathbf{T}_{\theta}) - P_r(I_f)\|_F. \quad (2)$$

We illustrate the process of computing the similarity measure in the low-rank space schematically in Fig. 1. Moreover, Fig. 2 shows that using components with very low rank, i.e., $\text{rank} = 5$, the consequent low-rank image is relatively similar to the clean image.

2.2 Low-rank projection

Singular value decomposition (SVD) can be a way to compute the low-rank components $P_r(I_m \circ \mathbf{T}_{\theta})$ and $P_r(I_f)$. For example, suppose the SVD of I is $I = U\Sigma V^{\top}$, then the low-rank component $P_r(I)$ can be obtained by calculating $U_r \Sigma_r V_r^{\top}$, where U_r is comprised of the first r -th columns of U , and V_r is comprised of the first r -th columns of V ; Σ_r is a diagonal matrix whose diagonal elements are the first r -th singular values.

We could construct the low-rank projection $P_r(I)$ in two ways, i.e., SVD of the warped moving $I_m \circ \mathbf{T}_{\theta}$ or SVD of the fixed image I_f . But we found that directly computing the low-rank component of $I_m \circ \mathbf{T}_{\theta}$ would make the network fail to back-propagate the gradients.

Therefore, we propose to build the low-rank projection P_r by only using the SVD of I_f . Concretely, since $U_r^{\top} I_f V_r = \Sigma_r$, we can construct the low-rank projection in the following form:

$$P_r(I) = U_r^{\top} I V_r. \quad (3)$$

Here, U_r and V_r come from SVD of image I_f . Then, for any I , the rank of $\mathbf{P}_r(I)$ is not larger than r , and can satisfy the constraint in the definition of \mathbf{P}_r (Section 2.1). With such a low-rank projection, the formula (2) can be converted to a new form as follow:

$$\hat{\mathcal{D}}_{\mathcal{R}}(\mathbf{I}_m \circ \mathbf{T}_\theta, \mathbf{I}_f) = \|U_r^\top(\mathbf{I}_m \circ \mathbf{T}_\theta)V_r - U_r^\top(\mathbf{I}_f)V_r\|_F = \|U_r^\top(\mathbf{I}_m \circ \mathbf{T}_\theta)V_r - \Sigma_r\|_F. \quad (4)$$

We illustrate the low-rank projection schematically in Fig. 1. We also visualize the low-rank projection $\mathbf{P}_r(\mathbf{I}_f)$ as a image in Fig. 2.

2.3 Registration network with low-rank representation

We employ a registration network which takes a noisy image pair as an input and estimates the DDF between the images, based on a 3D encoder-decoder-style architecture. To encourage a suitable smooth displacement, we leverage bending energy as a deformation regularization term. We combine the intensity-based measure with the weighted deformation regularization term as the loss function. Hence, an optimal registration can be obtained via the optimization of the following objective function:

$$\hat{\theta} \in \arg \min_{\theta \in \Theta} \hat{\mathcal{D}}_{\mathcal{R}}(\mathbf{I}_m \circ \mathbf{T}_\theta, \mathbf{I}_f) + \lambda \cdot \mathcal{R}(\mathbf{T}_\theta). \quad (5)$$

3 Experiments and Results

We demonstrated the registration effectiveness of our model by performing intra-modality pair-wise registration on two tasks, i.e., cardiac image registration and abdominal image registration. Both tasks were performed on the synthetic noisy datasets.

3.1 Material and experiment settings

Synthetic noisy datasets. The *synthetic noisy datasets* were obtained by adding two types of noise commonly found in medical images, i.e., spatially invariant additive white Gaussian noise (AWGN) and Rician noise (RN), to *clean*⁴ intensity images, from publicly available medical image datasets. Before adding noise, we employed intensity normalization to scale the intensity values to range [0,1].

Cardiac image registration was performed on the MM-WHS challenge dataset [30,31], which provides 40 labeled multi-modality whole-heart images from multiple sites, including 20 cardiac CT and 20 cardiac MRI. We selected 10 subjects from each modality as training images.

⁴ Here, we assumed that the challenge data was noise-free for registration. However, the cardiac and abdominal MRI images from challenges [14,30] have degraded quality, due to artifacts and other factors. Future work will study the issues.

Abdominal image registration was performed on two multi-organ segmentation challenge datasets, i.e., Multi-Atlas Labeling Beyond the Cranial Vault challenge and CHAOS challenge [14]. The former consists of 30 labeled images scanned using CT modality, from which 20 images were chosen in random for training. The latter consists of 20 labeled images scanned using MRI modality, from which 10 images were chosen in random for training.

Evaluation. We evaluated the noisy image registration by calculating the Dice score between the label of warped moving image and the label of fixed image. Cardiac image registration was evaluated by two substructures, i.e., myocardium (MYO) and left ventricle (LV), and abdominal image registration was evaluated by two organs i.e., right kidney (RK) and left kidney (LK). We evaluated differences between Regnet-LRR and other methods on the same noisy datasets by Wilcoxon signed rank test [27] with a significance threshold of $p < 0.05$.

Experiment settings. In both tasks, we implemented and trained the registration networks via TensorFlow [1] on an NVIDIA[®] RTX[™] 2080 Ti GPU. The registration modules of Regnet-LRR were adapted from the open-source code including VoxelMorph [3], label-reg [12], MvMM-Regnet [18], and DeepReg [8]. Since Regnet-LRR estimated the 3D DDFs of images, we employed the Batch-SVD technique to optimize the network parameters. The Batch-SVD module was adapted from the open-source code of ROnet [9], and the pre-processing module was adapted from the open-source code of MvMM-Regnet [18] and CF-distance method [28]. Moreover, the Adam optimizer [16] was adopted, with a learning rate bouncing between $1e-5$ and $1e-4$ to accelerate convergence [22].

An optimal rank number results in a suitable low-rank projection, which minimizes the negative effect of noise on the registration results. We set $r = 48$, $\sigma = 0.1$ as the default rank number and noise level, respectively. Here, σ denotes the standard deviation of AWGN and RN. Moreover, high-quality registration depends on an optimal weight of bending energy which guarantees the global smoothness of the deformations. To be balanced, we set $\lambda = 0.5$ as the default parameter of the regularization term.

We analyzed the registration effectiveness using different loss functions. For example, we performed the registrations on noisy images using NCC loss function, referred to as G-Noisy-NCC (for AWGN noise), R-Noisy-NCC (for RN noise), and compared them with the same loss function on clean images, named as Clean-NCC, and so did MSE loss function.

3.2 Task 1: intra-modality registration on noisy cardiac images

Registration was performed after noise was added to the clean data. This setting simulated a practical noisy image registration problem, in which registration of noisy images was more difficult than that of clean data.

As shown in Table 1, while the registration achieved excellent performance on clean data (Clean-MSE and Clean-NCC), its performance dropped in noisy

Table 1. Average substructure Dice (%) of CT-to-CT and MRI-to-MRI pair-wise cardiac registration, with * indicating statistically significant improvement of Regnet-LRR on noisy datasets given by a Wilcoxon signed-rank test ($p < 0.05$). Standard deviations are shown in parentheses.

Methods	CT-to-CT			MRI-to-MRI		
	MYO	LV	Avg.	MYO	LV	Avg.
Clean-MSE	78.8(5.4)	83.7(5.1)	81.3	70.2(5.2)	87.8(4.0)	79.0
Clean-NCC	75.6(11.1)	82.8(9.5)	79.2	67.2(9.6)	88.5(3.7)	77.9
G-Noisy-MSE	73.6(5.2)	77.8(4.8)	75.7	65.1(5.5)	86.0(4.7)	75.6
G-Noisy-NCC	67.8(10.7)	76.6(10.8)	72.2	65.3(10.8)	85.8(5.0)	75.6
G-Noisy-LRR	74.5(7.2)*	80.9(10.1)*	77.7	67.8(5.2)*	87.1(3.3)*	77.5
R-Noisy-MSE	73.9(5.4)	77.3(6.5)	75.6	66.1(6.5)	86.6(5.9)	76.4
R-Noisy-NCC	68.8(11.1)	77.0(10.0)	72.9	66.2(10.6)	83.0(6.9)	74.6
R-Noisy-LRR	75.6(7.4)*	82.2(10.5)*	78.9	68.5(4.9)*	87.2(3.6)*	77.9

cases. For example, due to negative effect of the AWGN noise, the average Dice of myocardium and left ventricle dropped from 79.2% to 72.2% using NCC loss function with respect to CT modality. Obviously, intensity-based registration methods had problems due to the negative effect of certain level of noise.

By contrast, with the noise-free low-rank representation, we observed better registration accuracy on noisy CT and MRI images. Moreover, our method outperformed both the MSE and NCC loss functions on noisy images, yielding substantial and consistent improvements on two cardiac substructures. Notably, Regnet-LRR attained evident improvements on challenging cardiac MRI images with Rician noise, where the shape of the myocardium was clearly irregular, reaching an average myocardium Dice of 68.5% compared with 66.1% (R-Noisy-MSE) and 66.2% (R-Noisy-NCC).

3.3 Task 2: intra-modality registration on noisy abdominal images

In this experiment, we evaluated the proposed method with respect to the abdominal datasets with both CT and MRI modalities. Since the left and right kidneys are separate organs on the abdominal image, we cropped them out for registration separately.

Table 2 compares the registration accuracy obtained by different loss functions on clean and noisy images. The intensity-based loss functions were less competitive on the noisy datasets than the clean datasets, e.g., the average Dice of G-Noisy-NCC on abdominal images in CT modality dropped from 83.0% to 70.0%. On the other hand, our framework achieved higher performance in pair-wise abdominal image registration on noisy datasets.

3.4 Ablation study

To better understand the effectiveness of the low-rank representation for noisy image registration, we compared it with different noise levels and rank

Table 2. Average organ Dice (%) of CT-to-CT and MRI-to-MRI pair-wise abdomen registration, with * indicating statistically significant improvement of Regnet-LRR on noisy dataset given by a Wilcoxon signed-rank test ($p < 0.05$). Standard deviations are shown in parentheses.

Methods	CT-to-CT			MRI-to-MRI		
	RK	LK	Avg.	RK	LK	Avg.
Clean-MSE	82.6(4.8)	84.6(3.9)	83.6	82.7(5.3)	80.0(8.7)	81.4
Clean-NCC	79.1(3.1)	86.9(2.9)	83.0	84.8(3.6)	83.1(7.6)	84.0
G-Noisy-MSE	78.9(5.1)	81.5(3.8)	80.2	80.6(4.9)	76.9(8.6)	78.8
G-Noisy-NCC	69.4(6.6)	70.5(5.7)	70.0	77.7(6.6)	78.2(5.7)	78.0
G-Noisy-LRR	82.1(4.4)*	83.2(7.9)*	82.7	83.8(4.0)*	80.1(8.8)*	82.0
R-Noisy-MSE	78.5(7.1)	81.7(6.2)	80.1	80.6(5.9)	78.1(9.1)	79.4
R-Noisy-NCC	70.9(6.8)	69.4(5.2)	70.2	79.0(5.0)	80.0(5.5)	79.5
R-Noisy-LRR	82.1(4.6)*	84.3(3.5)*	83.2	83.3(4.4)*	81.8(8.7)*	82.6

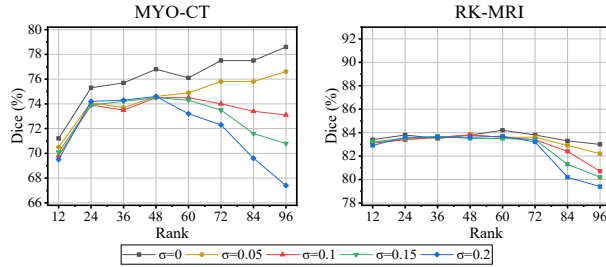


Fig. 3. Average substructure/organ Dice scores of pairwise labels using Regnet-LRR with σ noise levels and different rank numbers.

numbers. We added AWGN with specific noise levels, i.e., $\sigma \in [0, 0.2]$, and then made the rank number vary from 12 to 96. Fig. 3 reported the mean Dice scores, i.e., myocardium Dice with respect to CT modality (MYO-CT) and Dice of right kidney with respect to MRI modality (RK-MRI), obtained from Regnet-LRR.

The results clearly showed that the low-rank representation improved the robustness to noise with respect to intensity-based unsupervised registration models. When having a rank smaller than a specific threshold, i.e., $rank \leq 48$ for MYO-CT, and $rank \leq 72$ for RK-MRI, Regnet-LRR was insensitive to different noise levels. These results aimed to demonstrate that the low-rank representation can keep the image registration free from certain level of noise due to the advantages of image self-similarity.

However, we also observed growing sensitivity of the low-rank representation to the noise level as the rank increases. This discrepancy could be attributed to the incorporation of more high frequency information from the image as more intensity noises were also encompassed.

4 Conclusion

In this work, we propose a low-rank representation and formulate a novel loss function for the unsupervised registration network on noisy medical images. We have evaluated the proposed model on two tasks, i.e. cardiac and abdominal pair-wise registration based on three synthetic noisy datasets generated from publicly available medical image datasets. The proposed approach has shown its noise-free efficacy in registration on noisy medical images.

References

1. Abadi, M., Agarwal, A., Barham, P., Brevdo, E., Chen, Z., Citro, C., Corrado, G.S., Davis, A., Dean, J., Devin, M., Ghemawat, S., Goodfellow, I.J., Harp, A., Irving, G., Isard, M., Jia, Y., Józefowicz, R., Kaiser, L., Kudlur, M., Levenberg, J., Mané, D., Monga, R., Moore, S., Murray, D.G., Olah, C., Schuster, M., Shlens, J., Steiner, B., Sutskever, I., Talwar, K., Tucker, P.A., Vanhoucke, V., Vasudevan, V., Viégas, F.B., Vinyals, O., Warden, P., Wattenberg, M., Wicke, M., Yu, Y., Zheng, X.: Tensorflow: Large-scale machine learning on heterogeneous distributed systems. ArXiv [abs/1603.04467](https://arxiv.org/abs/1603.04467) (2015)
2. Ashburner, J., Brudfors, M., Bronik, K., Balbastre, Y.: An algorithm for learning shape and appearance models without annotations - sciencedirect. *Medical Image Analysis* **55**, 197–215 (2019)
3. Balakrishnan, G., Zhao, A., Sabuncu, M.R., Guttag, J.V., Dalca, A.V.: Voxel-morph: A learning framework for deformable medical image registration. *IEEE Transactions on Medical Imaging* **38**, 1788–1800 (2019)
4. Candès, E., Plan, Y.: Matrix completion with noise. *Proceedings of the IEEE* **98**(6), 925–936 (2010)
5. Candès, E., Recht, B.: Exact matrix completion via convex optimization. *Found. Comput. Math.* **9**(6), 717–772 (2009)
6. Dalca, A.V., Balakrishnan, G., Guttag, J.V., Sabuncu, M.R.: Unsupervised learning of probabilistic diffeomorphic registration for images and surfaces. *Medical image analysis* **57**, 226–236 (2019)
7. Dong, C., Loy, C., He, K., Tang, X.: Image super-resolution using deep convolutional networks. *IEEE Trans. Pattern Anal. Mach. Intell.* **38**(2), 259–307 (2016)
8. Fu, Y., Brown, N.M., Saeed, S.U., Casamitjana, A., Baum, Z.M.C., Delaunay, R., Yang, Q., Grimwood, A., Min, Z., Blumberg, S.B., Iglesias, J.E., Barratt, D.C., Bonmati, E., Alexander, D.C., Clarkson, M.J., Vercauteren, T., Hu, Y.: Deepreg: a deep learning toolkit for medical image registration. *Journal of Open Source Software* **5**(55), 2705 (2020)
9. Gao, S., Zhuang, X.: Rank-one network: An effective framework for image restoration. *IEEE Transactions on Pattern Analysis and Machine Intelligence* pp. 1–1 (2020)
10. Gu, S., Zhang, L., Zuo, W., Feng, X.: Weighted nuclear norm minimization with application to image denoising. In: *Proc. IEEE Conf. Compute. Vis. Pattern Recognit.* pp. 2862–2869 (2014)
11. Heinrich, M.P., Jenkinson, M., Bhushan, M., Matin, T., Gleeson, F.V., Brady, S.M., Schnabel, J.A.: MIND: Modality independent neighbourhood descriptor for multi-modal deformable registration. *Medical Image Analysis* **16**(7), 1423–1435 (2012)

12. Hu, Y., Modat, M., Gibson, E., Li, W., Ghavami, N., Bonmati, E., Wang, G., Bandula, S., Moore, C.M., Emberton, M., Ourselin, S., Noble, J.A., Barratt, D.C., Vercauteren, T.: Weakly-supervised convolutional neural networks for multimodal image registration. *Medical Image Analysis* **49**, 1–13 (2018)
13. John, A.: Symmetric diffeomorphic modeling of longitudinal structural mri. *Frontiers in Neuroscience* **6**, 197 (2012)
14. Kavur, A., Gezer, N., Barış, M., Aslan, S., Conze, P.H., Groza, V., Pham, D., Chatterjee, S., Ernst, P., Ozkan, S., Baydar, B., Lachinovk, D., Han, S., Pauli, J., Isensee, F., Perkonigg, M., Sathish, R., Rajan, R., Sheet, D., Selver, M.: Chaos challenge - combined (ct-mr) healthy abdominal organ segmentation. *Medical Image Analysis* (12 2020)
15. Khalil, A., Ng, S.C., Liew, Y.M., Lai, K.W.: An overview on image registration techniques for cardiac diagnosis and treatment. *Cardiology research and practice* (2018)
16. Kingma, D.P., Ba, J.: Adam: A method for stochastic optimization. *CoRR abs/1412.6980* (2014)
17. Lowe, D.G.: Distinctive image features from scale-invariant keypoints. *International Journal of Computer Vision* **60**(2), 91–110 (2004)
18. Luo, X., Zhuang, X.: Mvmm-regnet: A new image registration framework based on multivariate mixture model and neural network estimation. In: Martel, A.L., Abolmaesumi, P., Stoyanov, D., Mateus, D., Zuluaga, M.A., Zhou, S.K., Racoceanu, D., Joskowicz, L. (eds.) *Medical Image Computing and Computer Assisted Intervention – MICCAI 2020*. pp. 149–159. Springer International Publishing, Cham (2020)
19. Mikołajczyk, K., Schmid, C.: A performance evaluation of local descriptors. *IEEE Transactions on Pattern Analysis and Machine Intelligence* **27**(10), 1615–1630 (2005)
20. Schmidt, U., Roth, S.: Shrinkage fields for effective image restoration. In: *Proc. IEEE Conf. Compute. Vis. Pattern Recognit.* (2014)
21. Sedghi, A., O’Donnell, L.J., Kapur, T., Learned-Miller, E., Wells, W.M.: Image registration: Maximum likelihood, minimum entropy and deep learning. *Medical Image Analysis* **69**(518), 101939 (2020)
22. Smith, L.N.: Cyclical learning rates for training neural networks. 2017 IEEE Winter Conference on Applications of Computer Vision (WACV) pp. 464–472 (2015)
23. Sotiras, A., Davatzikos, C., Paragios, N.: Deformable medical image registration: A survey. *IEEE Transactions on Medical Imaging* **32**, 1153–1190 (2013)
24. Viergever, M.A., Maintz, J.B.A., Klein, S., Murphy, K., Staring, M., Pluim, J.P.W.: A survey of medical image registration - under review. *Medical image analysis* **33**, 140–144 (2016)
25. de Vos, B.D., Berendsen, F.F., Viergever, M.A., Sokooti, H., Staring, M., Išgum, I.: A deep learning framework for unsupervised affine and deformable image registration. *Medical Image Analysis* **52**, 128–143 (2018)
26. Wachinger, C., Navab, N.: Entropy and laplacian images: Structural representations for multi-modal registration. *Medical image analysis* **16**(1), 1–17 (2011)
27. Wilcoxon, F.: Individual comparisons by ranking methods. *biom. bull. Biometrics* **1**(6), 80–83 (1944)
28. Wu, F., Zhuang, X.: Cf distance: A new domain discrepancy metric and application to explicit domain adaptation for cross-modality cardiac image segmentation. *IEEE Transactions on Medical Imaging* **PP**(99), 1–1 (2020)
29. Zhuang, X., Arridge, S.R., Hawkes, D.J., Ourselin, S.: A nonrigid registration framework using spatially encoded mutual information and free-form deformations. *IEEE Transactions on Medical Imaging* **30**, 1819–1828 (2011)

30. Zhuang, X., Li, L., Payer, C., Štern, D., Urschler, M., Heinrich, M.P., Oster, J., Wang, C., Smedby, Ö., Bian, C., Yang, X., Heng, P.A., Mortazi, A., Bagci, U., Yang, G., Sun, C., Galisot, G., Ramel, J.Y., Brouard, T., Tong, Q., Si, W., Liao, X., Zeng, G., Shi, Z., Zheng, G., Wang, C., MacGillivray, T., Newby, D.E., Rhode, K.S., Ourselin, S., Mohiaddin, R., Keegan, J., Firmin, D.N., Yang, G.: Evaluation of algorithms for multi-modality whole heart segmentation: An open-access grand challenge. In: *Medical Image Analysis* (2019)
31. Zhuang, X., Shen, J.: Multi-scale patch and multi-modality atlases for whole heart segmentation of mri. *Medical image analysis* **31**, 77–87 (2016)